THE JOURNAL OF BIOLOGICAL CHEMISTRY VOL. 285, NO. 41, pp. 31559–31570, October 8, 2010

The Crystal Structure of Human Transketolase and New Insights into Its Mode of Action*

Received for publication, May 31, 2010, and in revised form, July 14, 2010 Published, JBC Papers in Press, July 28, 2010, DOI 10.1074/jbc.M110.149955

Lars Mitschke[‡1], Christoph Parthier[‡1], Kathrin Schröder-Tittmann[‡], Johannes Coy[§], Stefan Lüdtke[‡¶], and Kai Tittmann[‡¶2]

From the [‡]Institute of Biochemistry and Biotechnology, Martin-Luther-University Halle-Wittenberg, 06120 Halle, Germany, [§]TAVARGENIX GmbH, 64293 Darmstadt, Germany, and the [¶]Albrecht-von-Haller-Institute and Göttingen Center for Molecular Biosciences, Department of Bioanalytics, Georg-August-University Göttingen, D-37077 Göttingen, Germany

The crystal structure of human transketolase (TKT), a thiamine diphosphate (ThDP) and Ca^{2+}-dependent enzyme that catalyzes the interketol transfer between ketoses and aldoses as part of the pentose phosphate pathway, has been determined to 1.75 Å resolution. The recombinantly produced protein crystallized in space group C2 containing one monomer in the asymmetric unit. Two monomers form the homodimeric biological assembly with two identical active sites at the dimer interface. Although the protomer exhibits the typical three (α/β)-domain structure and topology reported for TKTs from other species, structural differences are observed for several loop regions and the linker that connects the PP and Pyr domain. The cofactor and substrate binding sites of human TKT bear high resemblance to those of other TKTs but also feature unique properties, including two lysines and a serine that interact with the β-phosphate of ThDP. Furthermore, Gln^{189} spans over the thiazolium moiety of ThDP and replaces an isoleucine found in most non-mammalian TKTs. The side chain of Gln^{428} forms a hydrogen bond with the 4′-amino group of ThDP and replaces a histidine that is invariant in all non-mammalian TKTs. All other amino acids involved in substrate binding and catalysis are strictly conserved. Besides a steady-state kinetic analysis, microscopic equilibria of the donor half-reaction were characterized by an NMR-based intermediate analysis. These studies reveal that formation of the central 1,2-dihydroxyethyl-ThDP carbanion-enamine intermediate is thermodynamically favored with increasing carbon chain length of the donor ketose substrate. Based on the structure of human transketolase and sequence alignments, putative functional properties of the related transketolase-like proteins TKTL1 and -2 are discussed in light of recent findings suggesting that TKTL1 plays a role in cancerogenesis.

Transketolase (TKT[3]; EC 2.2.1.1) is a ubiquitous enzyme in cellular carbon metabolism and requires thiamine diphosphate (ThDP), the biologically active derivative of vitamin B1, and Ca^{2+} ions as cofactors for enzymatic activity (1, 2). TKT catalyzes the reversible transfer of two-carbon (1,2-dihydroxyethyl) units from ketose phosphates to the C1 position of aldose phosphates and thus provides, together with the Schiff base-forming transaldolase, a reversible link between glycolysis and the pentose phosphate pathway. This shunt permits cells a flexible adaptation to different metabolic needs as the pentose phosphate pathway supplies intermediates for other metabolic pathways; generates precursors for biosynthesis of nucleotides, aromatic amino acids, and vitamins; and further produces NADPH for sustaining the glutathione level and for reductive biosynthetic pathways of, for example, cholesterol and fatty acids.

TKT acts on different ketose phosphate (donor) and aldose phosphate (acceptor) substrates of variable carbon chain length (3–7 carbons) in two major, essentially reversible reactions.

$$X5P + R5P \Leftrightarrow S7P + G3P$$

$$X5P + E4P \Leftrightarrow F6P + G3P$$

REACTIONS 1 AND 2

A simplified reaction scheme for the TKT-catalyzed conversion of substrates X5P and R5P into products S7P and G3P is shown in Fig. 1. The reaction cycle can be subdivided into a donor half-reaction (donor ligation and cleavage) and an acceptor half-reaction (acceptor ligation and product liberation) (3).

After formation of the reactive ylide form of ThDP, the C2 carbanion of ThDP attacks the carbonyl of donor X5P in a nucleophilic manner to yield the covalent donor-ThDP adduct X5P-ThDP (step 1). Ionization of C3-OH and cleavage of the scissile C2–C3 bond of X5P-ThDP results in the formation of product G3P and of the 1,2-dihydroxylethyl-ThDP (DHE-ThDP) carbanion/enamine intermediate (step 2). This intermediate may then react with either G3P (reverse reaction of step 2) or R5P in competing equilibria. In the latter case, C2α of DHE-ThDP ligates to C1 of R5P (in the acyclic form), yielding

* This work was supported by a grant from the "Fonds der Chemischen Industrie" (stipend to S. L.) and the Deutsche Forschungsgemeinschaft-funded Göttingen Graduate School for Neurosciences and Molecular Biosciences (to K. T.).

The atomic coordinates and structure factors (code 3MOS) have been deposited in the Protein Data Bank, Research Collaboratory for Structural Bioinformatics, Rutgers University, New Brunswick, NJ (http://www.rcsb.org/).

[1] Both authors contributed equally to this work.

[2] To whom correspondence should be addressed: Ernst-Caspari-Haus, Justus-von-Liebig-Weg 11, D-37077 Göttingen, Germany. Tel.: 49-551-3914430; Fax: 49-551-395749; E-mail: ktittma@gwdg.de.

[3] The abbreviations used are: TKT, transketolase; G3P, D-glyceraldehyde 3-phosphate; E4P, D-erythrose 4-phosphate; X5P, D-xylulose 5-phosphate; R5P, D-ribose 5-phosphate; F6P, D-fructose 6-phosphate; S7P, D-sedoheptulose 7-phosphate; ThDP, thiamine diphosphate; DHE-ThDP, 1,2-dihydroxyethyl-ThDP; X5P-ThDP, covalent adduct of X5P and ThDP; F6P-ThDP, covalent adduct of F6P and ThDP; S7P-ThDP, covalent adduct of S7P and ThDP.

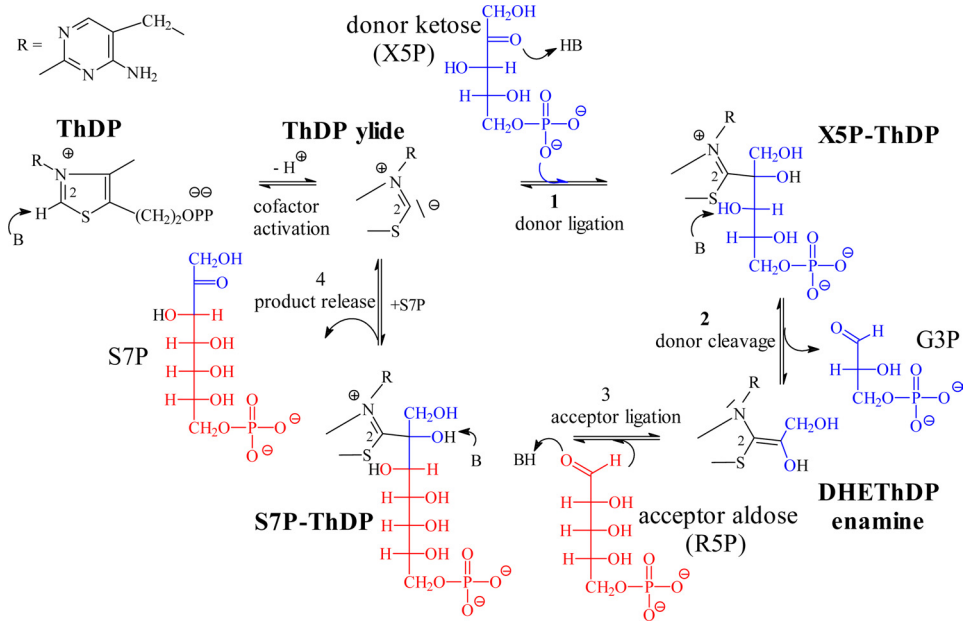

FIGURE 1. **Minimal reaction mechanism of TKT for the conversion of donor ketose X5P and acceptor aldose R5P into S7P and G3P with intermediates and elementary steps of catalysis identified.**

the covalent S7P-ThDP adduct (step 3). Eventual liberation of product S7P completes the reaction cycle (step 4).

TKTs from different species show a remarkably high degree of sequence similarity. Whereas the bacterial, yeast, and plant enzymes comprise about ~45–50% identical amino acids, mammalian TKTs share less identity with TKTs from other organisms (4). Human TKT shows ~27% sequence identity with TKT from yeast, *Escherichia coli* (tktA), and maize. Sequence analysis further revealed that ~50 amino acids are invariant across all species, including many residues shown to be involved in cofactor and substrate binding, such as a cluster of histidine and arginine residues. However, there are approximately 2 dozen residues that differ between the mammalian sequences and those of all other species. Most intriguingly, an active center histidine (His^{481} in yeast TKT) that is invariant in all non-mammalian TKTs is substituted by glutamine in the mammalian enzymes, ruling out the possibility that this residue acts as an acid/base catalyst (4, 5).

All TKTs characterized to date are homodimers related by a 2-fold rotational symmetry and consist of subunits of ~70–75 kDa (2). The V-shaped subunit consists of three α/β-type domains: the N-terminal PP domain, the middle PYR domain, and the C-terminal domain. Two identical active sites are formed at the dimer interface between the PP domain and the Pyr domain of the neighboring subunit. The biological function of the C-terminal domain is unknown.

The high resolution structures of TKT from yeast, *E. coli*, maize, *Thermus thermophilus*, and several pathogenic bacteria were determined by x-ray crystallography (6–9). In the case of the yeast and bacterial enzymes, crystallographic snapshots of reaction intermediates delineated the stereochemical course of substrate binding and processing (10–13). However, there is no structural information available for any mammalian TKT, including the human enzyme. Alterations in the activity of human TKT have been reported to cause and/or accompany different pathological disorders, including the Wernicke-Korsakoff syndrome, Alzheimer disease, or diabetes (14–16). Furthermore, TKT was suggested to be a critical determinant for impaired hippocampal neurogenesis, lymphatic metastasis of hepatocarcinoma, fibromyalgia, tumor cell growth, resistance of colon cancer toward 5-fluoruracil, and female fertility (17–21).

Mammalian TKT is expressed in all tissues highlighting its central metabolic function (22, 23). Interestingly, the highest expression level for TKT in mouse was found in cornea, where TKT amounts for ~10% of the total soluble protein, suggesting that it functions as an enzyme-crystallin (23). Furthermore, cumulative evidence was mounted that the vast majority of nucleic acid ribose in cancer cells is provided by the non-oxidative part of PPP through activity of TKT and transaldolase. In view of the central role of TKT in normal and different disease states, human TKT appears to be a promising drug target. In this context, it was previously demonstrated that the activity of human TKT could be effectively decreased both *in vivo* and *in vitro* by the addition of inactive cofactor analogues (24–27). There is also evidence of a direct correlation between impaired TKT activity and reduced cancer growth (24).

Besides TKT, the human genome encodes for two closely related proteins, which were termed TKTL1 and TKTL2 (transketolase-like proteins 1 and 2) (28). Human TKT shares a high sequence identity with both TKTL1 (61%) and TKTL2 (66%). However, a marked difference between TKT and TKTL1 is a deletion of 38 amino acids in the N-terminal PP domain (residues 76–113 in TKT), including 4 residues (Tyr^{83}, Gly^{90}, His^{110}, and Pro^{111}) that are totally invariant among all transketolase sequences (4). Recently, it was suggested that TKTL1 might play an important role for cancerogenesis, because numerous studies reported a direct correlation between the expression level of TKTL1 and invasion efficiency of cancer cells and the

corresponding mortality of patients (29). The biological function of TKTL2 is unknown.

Herein, we report on the newly determined crystal structure of human TKT as the first structure of a mammalian TKT. Structural differences between the human enzyme and its orthologs from yeast, bacteria, and plants are discussed. In addition, the macroscopic and microscopic kinetics of human TKT are studied by different assays. Finally, we hypothesize about the functional relationship of TKT and the proteins TKTL1 and TKTL2.

EXPERIMENTAL PROCEDURES

Reagents—Chemicals were purchased from Sigma-Aldrich, Carl Roth & Co., Merck, and AppliChem. Yeast extract for fed batch fermentation was purchased from Deutsche Hefewerke GmbH & Co. (Hamburg, Germany). Restriction enzymes were obtained from MBI Fermentas. Thrombin cleavage kit, TKT substrates (X5P, R5P, and β-hydroxypyruvate), and auxiliary enzymes triose-phosphate isomerase and *sn*-glycerol-3-phosphate:NAD^+ 2-oxidoreductase were from Sigma-Aldrich. Quartz double-distilled water was used throughout the experiments.

Chemoenzymatic Synthesis of S7P—The donor sugar S7P was chemoenzymatically synthesized, relying on the protocol given by Charmantray *et al.* (30) but using wild-type TKT from *E. coli*. In brief, TKT was reacted with artificial donor β-hydroxypyruvate and the physiological acceptor R5P, making the donor half-reaction irreversible. Correct synthesis and purity of S7P were confirmed by nanoelectrospray ionization mass spectrometry.

Cloning, Expression, and Purification of Human Transketolase—The cDNA encoding for human TKT was optimized for bacterial (*E. coli*) expression and synthesized by Geneart AG (Regensburg, Germany). The synthetic DNA was inserted into vector pET28a(+) using NcoI and XhoI restriction sites and transformed into *E. coli* strain Top 10. The plasmid DNA of the clones was isolated using the QIAprep Spin Miniprep kit. DNA sequence identity was confirmed by sequencing of the whole plasmid (Eurofins MWG Operon).

The final expression vector comprises an additional sequence encoding for a C-terminal thrombin cleavage site followed by a hexahistidine tag: 5′-pET 28a-NcoI-human TKT-(thrombin cleavage site)-XhoI-hexa-His-3′. This tag extends human TKT by an additional 14 amino acids at the C terminus, TKT-(Leu-Val-Pro-Arg-Gly-Ser-Leu-Glu)-(His-His-His-His-His-His) and 4 residues after thrombin cleavage, TKT-Leu-Val-Pro-Arg.

The pET28a(+) vector containing the *tkt* gene was transformed into *E. coli* $BL21C^+$ (Invitrogen) cells by electroporation. $BL21C^+$ cells containing the pET28a(+)-*tkt* plasmid were grown on LB plates containing 35 μg/ml kanamycin overnight at 37 °C. A single colony was then used to inoculate a 300-ml overnight culture (LB medium, 35 μg/ml kanamycin) for cell cultivation in a biofermenter (B. Braun Biotech) at 37 °C. The overnight culture was centrifuged (6000 rpm, 20 min, 4 °C), and the cell pellet was resuspended in 300 ml of LB medium containing 35 μg/ml kanamycin. This cell suspension was used to inoculate 6 liters of fermentation medium (300 g of yeast extract, 3 g of NH_4Cl, 30 g of glucose, 4 g of $MgSO_4$, 66 g of K_2HPO_4, 1 ml of antifoam) supplemented with 35 μg/ml kanamycin. The culture was stirred with 600–1500 rpm at a $p(O_2)$ of 100% at 37 °C. After depletion of the glucose, feeding was started using a glucose feeding solution (2 liters containing 600 g of yeast extract and 600 g of glucose). The air flow was gradually increased during feeding from 3 to 12 liters/min. A constant pH of 7 was maintained by automatic titration of 10% NaOH and 10% H_3PO_4. At an A_{600} of ~50, the temperature was rapidly decreased to 20 °C, and thiamine hydrochloride (70 μM) was added to the fermentation medium. Gene expression was induced by the addition of 100 μM IPTG. After 3 h of expression (A_{600} ~78), cells were pelleted by centrifugation (6000 rpm, 20 min, 4 °C). The cells (wet weight of ~1.1 kg) were stored at −70 °C until usage.

For purification, ~100 g of cells were thawed and resuspended on ice in 300 ml of buffer containing 25 mM Tris-HCl, pH 8.0, 300 mM NaCl, 20 mM imidazole, 1 mM $CaCl_2$, and 0.1 mM ThDP. In addition, DNase (5 μg/ml), $MgSO_4$ (1 mM), lysozyme (0.6 mg/ml), and PMSF (1 mM) were added. The suspension was then gently stirred on ice for 30 min. Cells were disrupted by three passages in a French press device. The cell debris was separated from the soluble fraction by ultracentrifugation (30,000 rpm, 45 min, 4 °C). The clear supernatant was then loaded onto a Ni^{2+}-NTA column previously equilibrated with 200 ml of 25 mM Tris-HCl, pH 8.0, 300 mM NaCl, 20 mM imidazole, 1 mM $CaCl_2$, and 0.1 mM ThDP. Human TKT was eluted from the column using a linear gradient (0–100%) elution buffer (25 mM Tris-HCl, pH 8.0, 300 mM NaCl, 200 mM imidazole, 1 mM $CaCl_2$) over a volume of 200 ml. Fractions containing TKT were pooled and loaded onto a G-25 HighPrep desalting column previously equilibrated with 50 mM glycyl-glycine (either pH 7.6 for functional analysis or pH 7.9 for crystallization). TKT was finally adjusted to a concentration of 20–30 mg/ml by ultrafiltration using microconcentrators (VIVASPIN, molecular weight cut-off of 30,000, 4000 rpm, 4 °C).

Thrombin Cleavage of C-terminal His_6 Tag—The C-terminal His_6 tag of TKT was cleaved off using the THROMBIN CleanCleave™ kit (Sigma-Aldrich). A volume of 1 ml of thrombin-agarose was applied per mg of TKT. Proteolytic digestion was carried out for 12 h at 20 °C. Afterward, the reaction mixture was centrifuged at 500 × *g* for 5 min at 20 °C. The supernatant containing processed TKT was separated from the agarose. The beads were washed again with 5 ml of 50 mM glycyl-glycine and recentrifuged at 500 × *g* for 5 min at 20 °C. The supernatant was added to that of the previous step and loaded onto a 1-ml Ni^{2+}-NTA column. Although unprocessed protein and His tag-containing peptides bind to the column, processed TKT passes the column and was only detected in the flow-through as judged by SDS-PAGE analysis.

Steady-state Kinetics Analysis—The enzymatic activity of human TKT (with and without His_6 tag) for conversion of X5P and R5P into S7P and G3P (Reaction 1) was determined in a spectrophotometric steady-state assay using the auxiliary enzymes triose-phosphate isomerase and *sn*-glycerol-3-phosphate:NAD^+ 2-oxidoreductase to detect formation of G3P, which derives from cleavage of X5P. The concomitant oxidation of NADH was followed spectrophotometrically at 340 nm in 50 mM glycyl-glycine, pH 7.6, at 30 °C. The assay further

contained 0.22 mM NADH, 3.6 units of *sn*-glycerol-3-phosphate:NAD^+ 2-oxidoreductase/triose-phosphate isomerase, 100 μM ThDP, 5 mM $CaCl_2$, 0.1–0.5 mg/ml human TKT, and variable concentrations of X5P and R5P. One unit is defined as the formation of 1 μmol of G3P/min. In order to determine the K_m values for X5P and R5P, the concentration of one substrate was kept constant at 2 mM. The dependence of the initial rates on the substrate concentration was analyzed according to the Michaelis-Menten equation.

The TKT activity in the so-called one-substrate reaction was analyzed using the same assay and conditions but in the presence of X5P as sole substrate (*i.e.* devoid of acceptor R5P). It could be demonstrated for TKTs from other organisms that X5P is slowly converted to G3P and erythrulose (carboligation product of two glycolaldehyde molecules) in the absence of an acceptor (31).

Analysis of Reaction Intermediates under Equilibrium Conditions by ^{1}H NMR Spectroscopy after Acid Quench Isolation—The donor half-reactions of human TKT with donor ketoses X5P, F6P, and S7P were analyzed by one-dimensional ^{1}H NMR spectroscopy after acid quench isolation of reaction intermediates (12, 32). This approach allows us to quantitatively assess the microscopic equilibria of the donor half-reaction comprising formation of (i) the substrate Michaelis complex (K_1), (ii) the covalent donor-ThDP adduct (X5P-ThDP, F6P-ThDP, S7P-ThDP) (K_2), and (iii) cleavage of the latter intermediate into DHE-ThDP and an aldose phosphate product (K_3) as shown below.

$$E\text{-ThDP} + \text{donor (X5P/F6P/S7P)} \overset{K_1}{\Longleftrightarrow} E\text{-ThDP} * \text{donor (Michaelis complex)} \overset{K_2}{\Longleftrightarrow} \text{covalent donor-ThDP adduct} \overset{K_3}{\Longleftrightarrow} E\text{-DHE-ThDP} + \text{product (G3P/E4P/R5P)}$$

REACTION 3

The relative concentrations of the intermediates were estimated by ^{1}H NMR spectroscopy using the C2-H signal of ThDP (9.70 ppm) and the C6′-H proton signals of chemically synthesized DHE-ThDP (7.31 ppm), and of chemoenzymatically synthesized X5P-ThDP (7.35 ppm) and F6P-ThDP (7.34 ppm) adducts as standards. As shown under "Results and Discussion," the covalent S7P-ThDP intermediate could be detected and assigned for the first time in this study.

In a typical experiment, 15 mg/ml holoenzyme (219 μM active sites) in 50 mM glycyl-glycine, pH 7.6, was mixed with 50 mM substrate solution (X5P, F6P, or S7P in the same buffer) in a 1 + 1 mixing ratio (200 μl each) for 30 s at 30 °C. The reaction was then stopped by the addition of 200 μl of TCA/HCl as detailed (32). NMR data acquisition and processing were performed as described previously (32).

Crystallization of Human TKT—Human transketolase bearing a C-terminal His_6 tag was successfully crystallized by the hanging drop vapor diffusion method. Remarkably, all attempts to crystallize thrombin-processed TKT (devoid of His tag) failed. For initial crystallization trials, we relied on conditions established for crystallization of TKTs from *E. coli* and *S. cerevisiae* (8, 33). The quality of these initially obtained crystals was not sufficient for an x-ray structural analysis. In order to improve the crystal quality, several additive screens were tested. These optimization trials revealed a reservoir mixture of 13.5–15% (w/v) PEG 6000, 4% (v/v) PEG 400, and 2% (v/v) glycerol in 50 mM glycyl-glycine, pH 7.9, to be most suitable for a reproducible crystallization of single crystals of human TKT. To set up crystallization, 3 μl of protein solution (8–12 mg/ml, 0.6 mM ThDP, 5 mM $CaCl_2$ in 50 mM glycyl-glycine, pH 7.9) were mixed with 3 μl of the reservoir solution. Droplets were allowed to equilibrate with 500 μl of mother liquor at 8 °C. Crystal growth occurred within 3–5 days.

Data Collection, Structure Determination, and Refinement—Single crystals of human TKT were mounted to nylon cryoloops (Hampton Research) and transferred to cryoprotectant solution containing 20% (w/v) PEG 6000, 30% (v/v) ethylene glycol, 5 mM ThDP, 10 mM $CaCl_2$ in 50 mM glycyl-glycine, pH 7.9. After an incubation time of ~10 s, crystals were immediately flash-cooled by direct immersion into liquid nitrogen and transferred to the goniometer head.

A data set of a single crystal was collected in house in a 100 K nitrogen cryostream (XSTREAM2000, Rigaku/MSC, Japan) using copper Kα radiation (λ = 1.5418 Å) with an R-AXIS IV^{++} image plate detector (Rigaku/MSC, Japan) on a Rigaku MicroMax 007 rotating anode generator. The diffraction data extended to a resolution of 1.75 Å. Oscillation images were integrated, merged, and scaled using the XDS program package (34). Molecular replacement was carried out with Phaser using data from 20 to 1.75 Å and using a monomer of transketolase from *Saccharomyces cerevisiae* as a search model (Protein Data Bank code 1TRK) (35). Human transketolase crystallized in the monoclinic space group C2 with one monomer in the asymmetric unit forming half of the biologically functional dimer. The structure was manually rebuilt and verified against $2F_o - F_c$ electron density maps using Coot (36). Refinement was carried out with Refmac5, applying overall anisotropic B-factor and bulk solvent correction (35). Ligands and water molecules were added to the model at a late stage of refinement. The crystallographic *R*-factor was used to monitor the stage of refinement omitting 5% of the structure factors for calculation of R_{free}. The final model consists of residues 3–618 (human TKT comprises 623 residues), 1 ThDP molecule, 1 Ca^{2+} ion, 1 Na^+ ion, 10 1,2-ethanediol molecules, and 488 waters and was refined to R_{work} and R_{free} values of 0.169 and 0.205, respectively. The stereochemistry of the model was assessed by MolProbity (37). Preparation of the crystallographic images was carried out with PyMOL (the PyMOL Molecular Graphics System, Version 0.99, Schrödinger, LLC). Sequences were aligned with ClustalW2, and sequence figures were generated with ESPript 2.2 (38, 39).

RESULTS AND DISCUSSION

Previous studies had revealed that a heterologous expression of human TKT in bacterial hosts resulted in poor yields due to very modest expression levels, which allowed a functional characterization but did not provide sufficient amounts for crystallization and eventual x-ray structural analysis (40). Here, a syn-

TABLE 1
Steady-state kinetic constants of recombinantly expressed and native human TKT
Assay conditions are detailed under "Experimental Procedures."

	A_{spec}	k_{cat}	K_m(X5P)	K_m(R5P)
	units/mg	s^{-1}	μM	μM
Recombinant human TKT-His_6 (30 °C, this study)	2.7 ± 0.1	3.1 ± 0.1	303 ± 79	610 ± 36
Recombinant human TKT (30 °C, this study)	5.5 ± 0.1	6.3 ± 0.1	255 ± 37	480 ± 41
Recombinant human His_6-TKT (37 °C)[a]	13.5	15.5	270 ± 20	510 ± 50
Native human TKT (37 °C)[a]	12–17	14–19	490 ± 140	530 ± 40

[a] Data from Ref. 1.

thetic codon-optimized *tkt*-cDNA was expressed in *E. coli* $BL21C^+$ cells under high cell density conditions in a biofermenter. Approximately 40–50 mg of human TKT bearing a C-terminal His_6 tag and a preceding thrombin cleavage site were purified to homogeneity from 100 g of cells. The His_6 tag could be quantitatively removed by thrombin digestion.

The activity of human transketolase with and without the C-terminal His tag was determined relying on a coupled assay with auxiliary enzymes triose-phosphate isomerase and G3PDH to monitor conversion of donor X5P and acceptor R5P into products G3P and S7P. The activity of human TKT is not dependent on the presence of excess ThDP and Ca^{2+} in the assay mixture, indicating that the as isolated form of the protein is fully saturated with cofactors paralleling earlier observations (40). This quasi-irreversible cofactor binding is a marked difference between the human enzyme and bacterial or yeast TKT, which bind ThDP and Ca^{2+} in a reversible manner. The steady-state kinetic constants of recombinantly produced human TKT (Table 1) are in fair agreement with the reported values for material purified from native sources or obtained by recombinant expression using an N-terminal His_6 tag. Under the chosen experimental conditions (pH 7.6, 30 °C), the His-tagged protein exhibits a specific activity of 2.7 ± 0.1 units/mg and K_m values of 610 ± 36 μM for R5P and 303 ± 79 μM for X5P. Both the specific activity and substrate affinity of TKT after His tag removal are slightly increased and amount to 5.5 ± 0.1 units/mg, 480 ± 41 μM (K_m for R5P), and 255 ± 37 μM (K_m for X5P). This result indicates that the C-terminal His tag slightly impairs substrate binding and catalysis.

Kinetic analysis of the one-substrate reaction (depletion of X5P in the absence of R5P) revealed a maximal activity of 0.68 ± 0.09 unit/mg and a K_m^{app} for X5P of 6.3 ± 1.6 mM (data not shown). At a concentration of 2 mM X5P, the observed activity of 0.14 unit/mg corresponds to a mere 2.8% activity of the native reaction (~5 units/mg, 2 mM X5P and R5P).

Analysis of Reaction Intermediates under Equilibrium Conditions by ^{1}H NMR Spectroscopy after Acid Quench Isolation—When TKT is reacted with a donor ketose (X5P, F6P, or S7P), the donor half-reaction comprising three reversible reaction steps and four different enzyme states (Reaction 3) will settle to equilibrium and stall halfway the catalytic cycle (3, 13). Because we have employed saturating substrate concentration of 25 mM in each case, the fraction of free enzyme is negligible under these conditions. Hence, three different catalytic states of the enzyme are mainly populated in sequential equilibria: (i) the substrate Michaelis complex, (ii) the covalent donor-ThDP adduct, and (iii) the DHE-ThDP carbanion/enamine (detected as the conjugate acid in the NMR experiments).

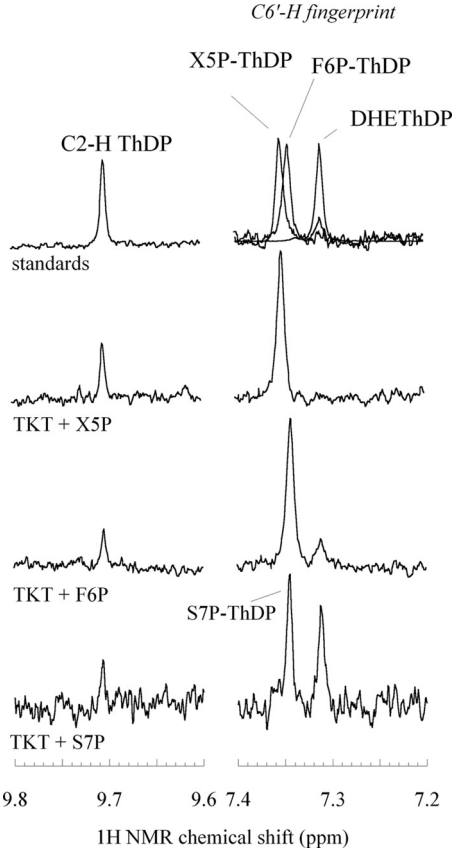

FIGURE 2. **^{1}H NMR-based analysis of the intermediate distribution at equilibrium after reaction of human TKT with saturating concentrations of either X5P, F6P, or S7P and subsequent acid quench isolation using the characteristic C2-H and C6′-H proton signals of ThDP and of chemically or chemoenzymatically synthesized intermediates as standards.** Due to acid quench isolation of reaction intermediates, the conjugate acid of the DHE-ThDP carbanion/enamine intermediate that is the C2α protonated form is detected.

The comparative quantitative analysis of reaction intermediates by ^{1}H NMR after acid quench isolation reveals clear differences in the equilibrium positions (K_2 and K_3 in Reaction 3) for the donor half-reactions of human TKT when employing alternative donor substrates X5P, F6P, and S7P (Fig. 2 and Table 2). In the presence of 25 mM X5P, ~75% of active sites are occupied with the covalent X5P-ThDP intermediate, and 25% of active sites contain C2-unsubstituted ThDP as a reporter for the substrate Michaelis complex. The fraction of the DHE-ThDP intermediate is too small (<5% active sites) to allow a reliable quantitation by NMR spectroscopy. When human TKT is reacted with 25 mM F6P, however, we observe a fraction of ~12% DHE-ThDP along with ~72% F6P-ThDP and ~16% ThDP (Michaelis complex). The fraction of DHE-ThDP

TABLE 2

Quantitative distribution of reaction intermediates in the donor half-reaction of human TKT under equilibrium conditions as estimated by ^{1}H NMR spectroscopy after acid quench isolation

Note that the conjugate acid of the DHE-ThDP carbanion/enamine intermediate is detected by NMR spectroscopy.

Donor substrate	C2-unsubstituted ThDP	Donor-ThDP adduct	DHE-ThDP
	%	%	%
X5P	25	75	<5
F6P	16	72	12
S7P	10	50	40

is even higher in the presence of saturating amounts of S7P. Here, ~40% of active sites contain DHE-ThDP, and 50% of active sites are occupied with the S7P-ThDP adduct and 10% with ThDP. It has to be noted that we do not have a chemical standard for an unequivocal assignment of the S7P-ThDP adduct by ^{1}H NMR, but the chemical reaction and the NMR spin system suggest that the singlet signal at 7.35 ppm originates from the latter intermediate.

Two main conclusions can be drawn from our studies. First and foremost, the fraction of the DHE-ThDP carbanion/enamine intermediate under true equilibrium conditions is dependent on the carbon chain length of the donor ketose substrate. Although this intermediate is not (donor X5P) or barely (donor F6P) detectable for 5- or 6-carbon substrates, there is a substantial fraction accumulated in the case of 7-carbon substrate S7P. The different equilibrium position between the covalent donor-ThDP adduct on one hand and the DHE-ThDP carbanion/enamine and aldose product on the other (K_3 in Reaction 3) (Reactions 4–6) could either result from a different reactant state stabilization of the respective donor-ThDP intermediates relative to the common DHE-ThDP carbanion/enamine intermediate or, alternatively, from different affinities of TKT for the aldose acceptor (G3P, E4P, or R5P) formed upon cleavage of the donor-ThDP adduct.

$$\text{X5P: } E\text{-X5P-ThDP} \overset{K_3}{\Leftrightarrow} E\text{-DHE-ThDP} + \text{G3P}$$

$$\text{F6P: } E\text{-F6P-ThDP} \Leftrightarrow E\text{-DHE-ThDP} + \text{E4P}$$

$$\text{S7P: } E\text{-S7P-ThDP} \Leftrightarrow E\text{-DHE-ThDP} + \text{R5P}$$

REACTIONS 4–6

The latter scenario appears unlikely because TKT exhibits a high affinity for R5P and E4P with K_m values in the submillimolar range, whereas G3P is a poor substrate with K_m in the lower millimolar range. Hence, one would expect the largest fraction of DHE-ThDP in the case of X5P, which is clearly not the case. Second, the fraction of C2-unsubstituted ThDP as a quantitative measure of the Michaelis complex decreases with increasing carbon chain length of the donor substrate (*i.e.* the largest fraction is observed for X5P as substrate, indicating a stronger reactant state stabilization in the case of this substrate relative to F6P and S7P).

Crystal Structure of Human TKT and Comparison with Orthologs from Different Species—The crystal structure of human TKT bearing a C-terminal His_6 tag has been determined by molecular replacement phasing using the structure of yeast TKT (Protein Data Bank code 1TRK) as search model and was refined to an R_{work}/R_{free} of 0.169/0.205 against data to 1.75 Å resolution (Table 3). The protein crystallized in space group C2, comprising one monomer in the crystallographic asymmetric unit. Two monomers form the biologically functional homodimer with C2 symmetry (Fig. 3*A*). Each subunit comprises in total 623 residues plus 14 additional residues of the C-terminal His tag, of which residues 3–618 are well defined by their electron density maps. The first 2 N-terminal and the last 5 C-terminal native residues as well as the His tag could not be traced, indicating these parts to be flexible. The final model of the asymmetric unit comprises 616 amino acids, one thiamine diphosphate and Ca^{2+} ion as cofactors, one Na^+ ion, and 10 ethanediol and 488 water molecules. The temperature factors of enzyme-bound ThDP (average *B*-value of 12.5 Å^2) are comparable with those of neighboring protein residues, indicating full occupancy with cofactor (Table 3).

TABLE 3

Crystallographic statistics

Values for the highest resolution shell (1.85-1.75 Å) are given in parentheses.

Parameter	Value
Data collection	
Wavelength (Å)	1.5418
Beamline	Home source (rotating anode)
Space group	C2
Cell dimensions	
a (Å), *b* (Å), *c* (Å)	113.63, 85.33, 72.74
β (degrees), $\alpha = \gamma = 90°$	125.7
Resolution (Å)	20-1.75 (1.85-1.75)
R_{merge}	5.0 (39.4)
R_{meas}	6.3 (49.4)
$I/\sigma I$	14.8 (2.8)
Completeness (%)	98.9 (96.2)
Redundancy	2.5 (2.4)
B-Factor from Wilson plot (Å^2)	27.5
Refinement	
Resolution (Å)	20-1.75
No. of reflections (work/test set)	53,132/2796
R_{work}	16.9
R_{free}	20.5
No. of atoms	
Protein	4730
Ligands	68
Water	488
Average *B*-factors (Å^2)	
Protein	20.2
ThDP	12.5
1,2-Ethanediol	25.9
Water	31.7
Root mean square deviations	
Bond lengths (Å)	0.014
Bond angles (degrees)	1.44
Ramachandran plot (%)	
Favored	98.2
Allowed	99.8
Molprobity Clashscore, all atoms	4.7

The two active sites of the TKT homodimer are formed at the interface of two neighboring subunits and are deeply buried at the bottom of a funnel-shaped substrate channel of ~14–16 Å in length and a width of 10–12 Å at the entrance and 7–9 Å at the interior (Fig. 3*B*). It is noteworthy that the substrate channels in all other structurally characterized non-mammalian TKTs are markedly wider than that of the human enzyme, providing a rationale for the broader substrate range of the non-mammalian enzymes (1, 7, 9, 41). In the resting state, the reactive C2 atom of the thiazolium portion and the 4-amino group of the aminopyrimidine are solvent-accessible. The entrance to

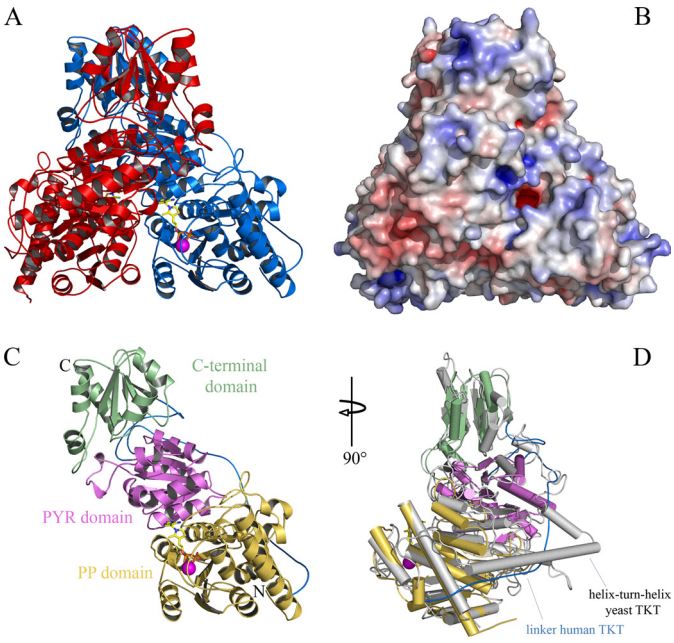

FIGURE 3. **Crystal structure of human TKT.** *A*, structure of the TKT dimer with bound cofactors ThDP (*yellow*) and Ca^{2+} (*magenta*) in a *schematic representation*. The individual subunits are shown in *blue* and *red*, respectively. *B*, *surface representation* of TKT dimer in the same orientation as in *A*. The surface electrostatic potential is *color-coded*, representing electrostatic potentials from −7 (*red*) to +7 (*blue*) k_BT. The surface potential was calculated with the APBS plugin of PyMOL. *C*, domain structure of TKT subunit in a *schematic representation* showing the three domains in a different *color code*: N-terminal PP domain in *yellow*, middle Pyr domain in *magenta*, and C-terminal domain in *green*. The monomer is shown in the same orientation as in *A*. *D*, superposition of subunits from human TKT (same *color code* as in *C*) and TKT from yeast (*gray*; Protein Data Bank code 1TRK) in a *schematic representation*. The structures are rotated ~90° around the 2-fold symmetry axis compared with previous panels.

the active site is lined with positively charged residues (Fig. 3*B*), which are presumably involved in binding of the substrates' phosphate moiety, whereas the substrate channel and the active site are negatively charged. The surface of human TKT is mostly uncharged but contains several acidic and basic patches.

In accordance with all previously determined TKT structures, the V-shaped subunit of human TKT folds into three consecutive α/β-type domains: the N-terminal PP domain that binds the pyrophosphate part of ThDP (residues 1–276), the Pyr domain that contacts the aminopyrimidine portion of ThDP (residues 316–472), and the C-terminal domain (residues 493–623) (Fig. 3*C*). The three domains are interconnected by flexible linker regions (PP-Pyr domains, residues 277–315; Pyr-C-terminal domains, residues 473–492) that do not adopt a defined secondary structure. The active site is constituted from multiple loops originating from the PP domain and the Pyr domain of two neighboring subunits, explaining the dimeric nature of the enzyme.

The PP domain consists of a central five-stranded parallel β-sheet structure with $\beta1$ $\beta2$ $\beta3$ $\beta5$ $\beta4$ topology surrounded by helices on both sides of the sheet. The Pyr domain comprises a parallel six-stranded β-sheet with $\beta7$ $\beta6$ $\beta8$ $\beta9$ $\beta11$ $\beta10$ topology and three helices on each side. Finally, the C-terminal domain is constituted by one antiparallel strand ($\beta12$) and four parallel strands ($\beta14$ $\beta13$ $\beta15$ $\beta16$) embedded into multiple helices. *B*-Factors indicate that the C-terminal domain exhibits the highest flexibility in the crystalline state (data not shown).

Both subunit and domain topology as well as the overall fold of human TKT are highly similar to those of yeast and bacterial TKT (Figs. 3*D* and 4). The subunits from the human and yeast enzyme can be superimposed with a root mean square deviation value of 2.1 Å and a high Dali *Z* score of 37.5 (579 Cα atoms were aligned) using the DaliLite version 3 program (42). A striking structural difference locates to the linker region between the PP and Pyr domains (Fig. 3*D*). Although this region is unstructured in human TKT, the corresponding segment in yeast TKT, which is ~20 amino acids longer, folds into a helix-turn-helix motif. In addition, the orientation of several helices in all three domains is slightly different. Remarkably, the spatial orientation of the central β-sheets in all three domains is almost identical in the two enzymes. Due to numerous gaps in the human TKT sequence when aligned to the yeast enzyme, several loops in the human enzyme are shorter or completely missing (Fig. 4).

As alluded to before, the active site containing the non-covalently bound cofactors ThDP and Ca^{2+} is formed at the interface between the PP and Pyr domains of both subunits. ThDP is held in place by numerous hydrogen bonding and hydrophobic interactions with the protein and by bonding of its diphosphate to the Ca^{2+} ion that is further coordinated by the protein main chain and several side chains (Fig. 5). ThDP adopts the canonical V-type conformation, which juxtaposes the catalytic 4′-NH_2 group of the aminopyrimidine and the reactive C2 of the thiazolium. The diphosphate moiety of ThDP is exclusively bound by the PP domain at the C-terminal ends of strands $\beta1$ and $\beta2$. The β-phosphate interacts with the side chains of residues Ser^{40}, Lys^{75}, His^{77}, Asn^{185}, and Lys^{244}. The α-phosphate contacts the backbone amides of Gly^{156} and Glu^{157}. The Ca^{2+} ion is coordinated by the α- and β-phosphate of ThDP, by the side chains of Asp^{155} and Asn^{185}, and by the backbone carbonyl of Leu^{187}. In addition, a water interacts with the β-phosphate, the Ca^{2+} ion, and several amino acid residues. Although the metal binding site comprising the GDG consensus sequence is strictly conserved in all TKTs (4, 43), mammalian TKTs have apparently evolved unique interactions with ThDP, including residues Ser^{40}, Lys^{77}, and Lys^{244}.

The side chain of Gln^{189} spans over the *re*-face of the thiazolium ring, whereas Leu^{125} is located at the opposite face and serves as a fulcrum, over which the methylene bridge that links the thiazolium and aminopyrimidine rings is bent. Furthermore, His^{258} is bound in close vicinity to the thiazolium and is presumably involved in substrate binding and catalysis. The N1′ atom of the aminopyrimidine is in hydrogen-bonding interaction with Glu^{366} of the Pyr domain, a conserved residue found in all ThDP enzymes except for glyoxylate carboligase. The 4′-NH_2 group of the aminopyrimidine contacts the backbone carbonyl of Gly^{123} (PP domain) and the side chain of Gln^{428} (Pyr domain). In addition, the aminopyrimidine rings interacts with the aromatic side chains of Phe^{389} and Phe^{392}, the latter bound in a π-stacking arrangement.

Recent crystallographic studies on several non-covalent and covalent reaction intermediates in TKT from *E. coli* and yeast as well as functional analysis of mutant proteins allowed the

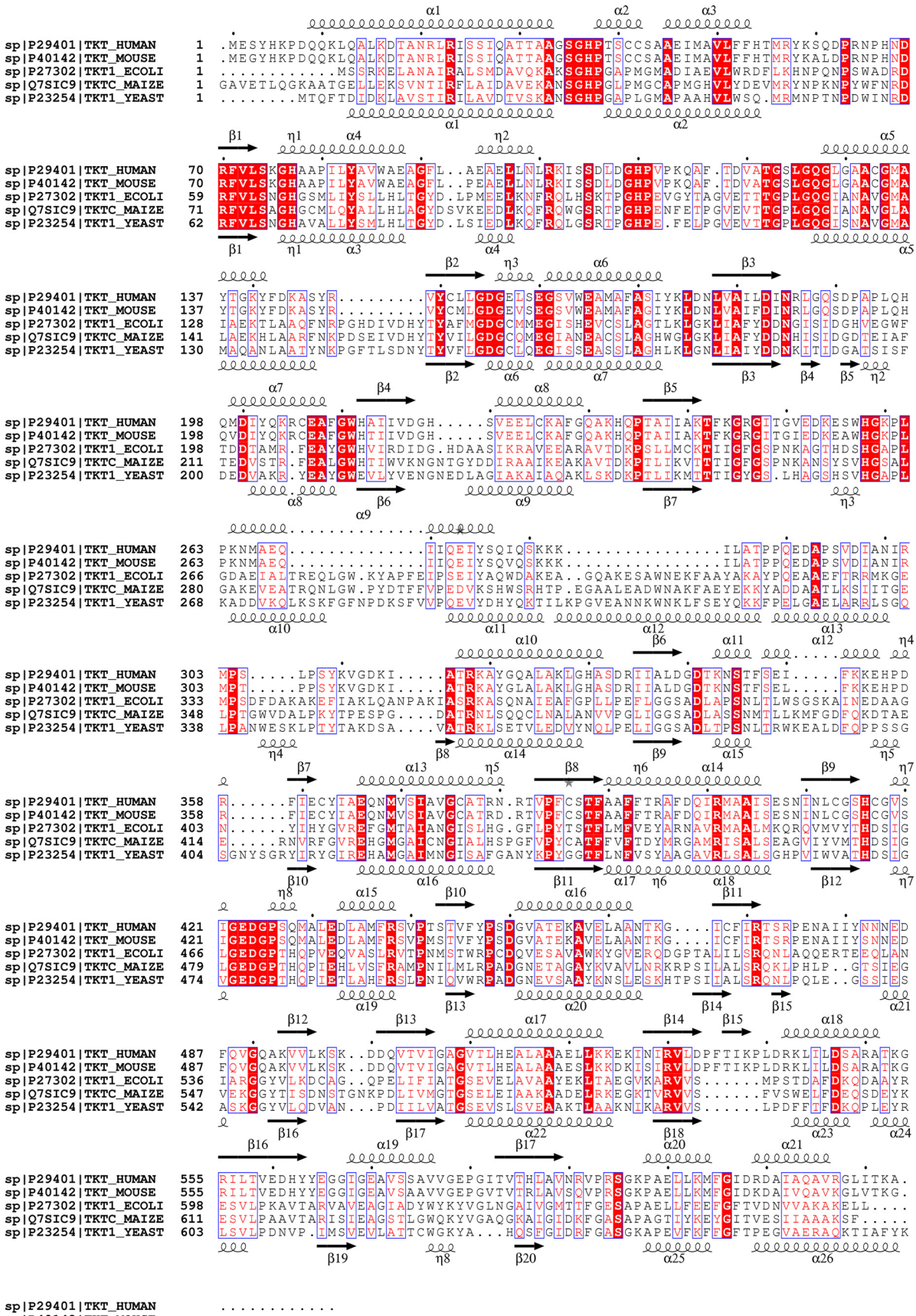
sp|P29401|TKT_HUMAN
sp|P40142|TKT_MOUSE
sp|P27302|TKT1_ECOLI
sp|Q7SIC9|TKTC_MAIZE
sp|P23254|TKT1_YEAST

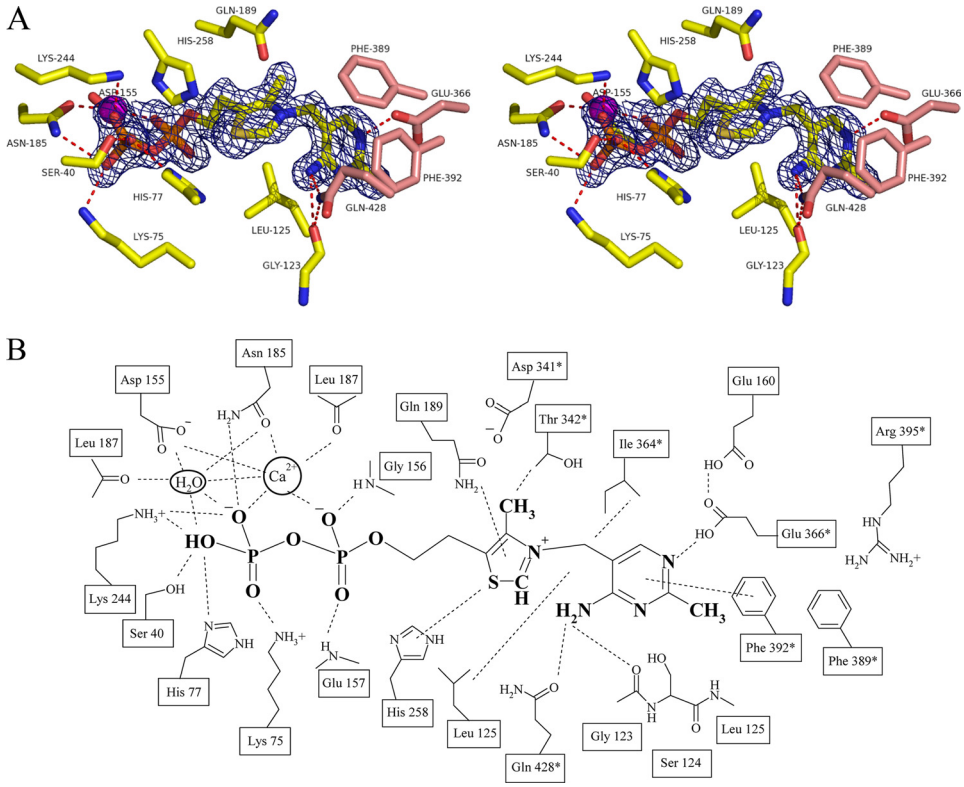

FIGURE 5. **Structure of the cofactor binding site in human TKT.** *A*, *stereo drawing* showing cofactor ThDP and selected amino acid residues in *stick representation* and Ca^{2+} as a *magenta sphere*. Amino acids contributed by different subunits are indicated by *different color-coding*. The final $2F_o - F_c$ electron density map of ThDP is contoured at 1.0σ. *B*, *schematic diagram* of the interactions of bound ThDP and Ca^{2+} at the active site of human TKT. Possible hydrogen-bonding and hydrophobic interactions are indicated by *dashed lines*. Residues from the neighboring subunit are indicated by an *asterisk*.

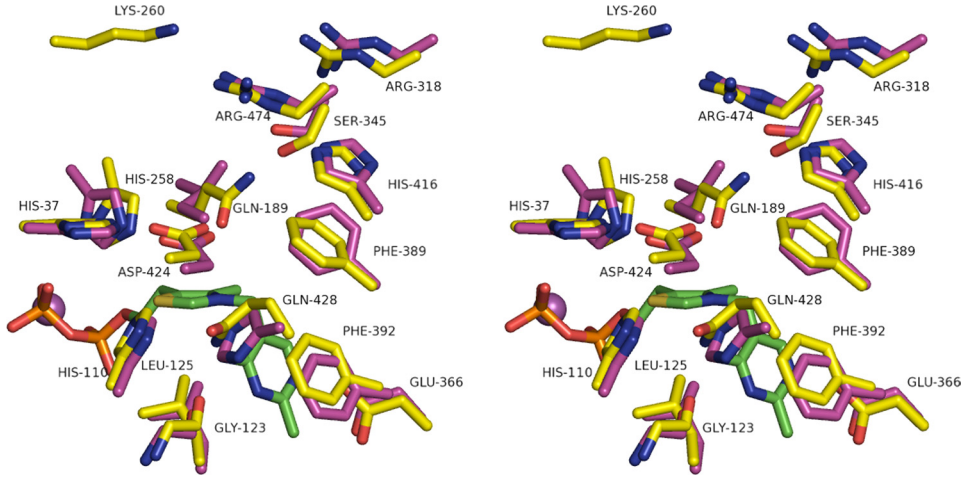

FIGURE 6. **Superposition of the active sites of human (*yellow*) and *E. coli* (*purple*) TKT in *stereo view* showing selected amino acid residues and bound ThDP (*green*) in *stick representation* and Ca^{2+} as a *magenta sphere*.** Residues of human TKT are labeled.

identification of critical interactions between the substrate/intermediates and the protein (10–12). A superposition of the active sites of human and *E. coli* TKT (Fig. 6) reveals that most of the active site residues are strictly conserved and occupy almost identical positions in the two proteins, including two arginines (Arg^{474} and Arg^{318} in human TKT), a serine (Ser^{345}), and a histidine (His^{461}) all shown to be involved in binding of the phosphate portion of the substrates. The same observation holds true for a cluster of histidines (His^{110}, His^{37}, His^{258}) and Asp^{424}, which are likely to form hydrogen bonds with the substrate hydroxyl groups, as shown for the homologous residues in bacterial TKT. Despite these commonalties, the human enzyme exhibits some unique features. Most intriguingly, Gln^{428} replaces a histidine (His^{481} in yeast TKT, His^{473} in *E. coli*

FIGURE 4. **Sequence alignment of human TKT *versus* orthologs from mouse, *E. coli*, maize, and yeast using the programs ClustalW2 and ESPript 2.2.** *Numbering* corresponds to the sequence of human TKT. Identical residues are indicated by a *red background*, and conserved residues are indicated by *red characters*. The secondary structure elements of human TKT are shown *above* the sequences, and those of yeast TKT are shown *below*.

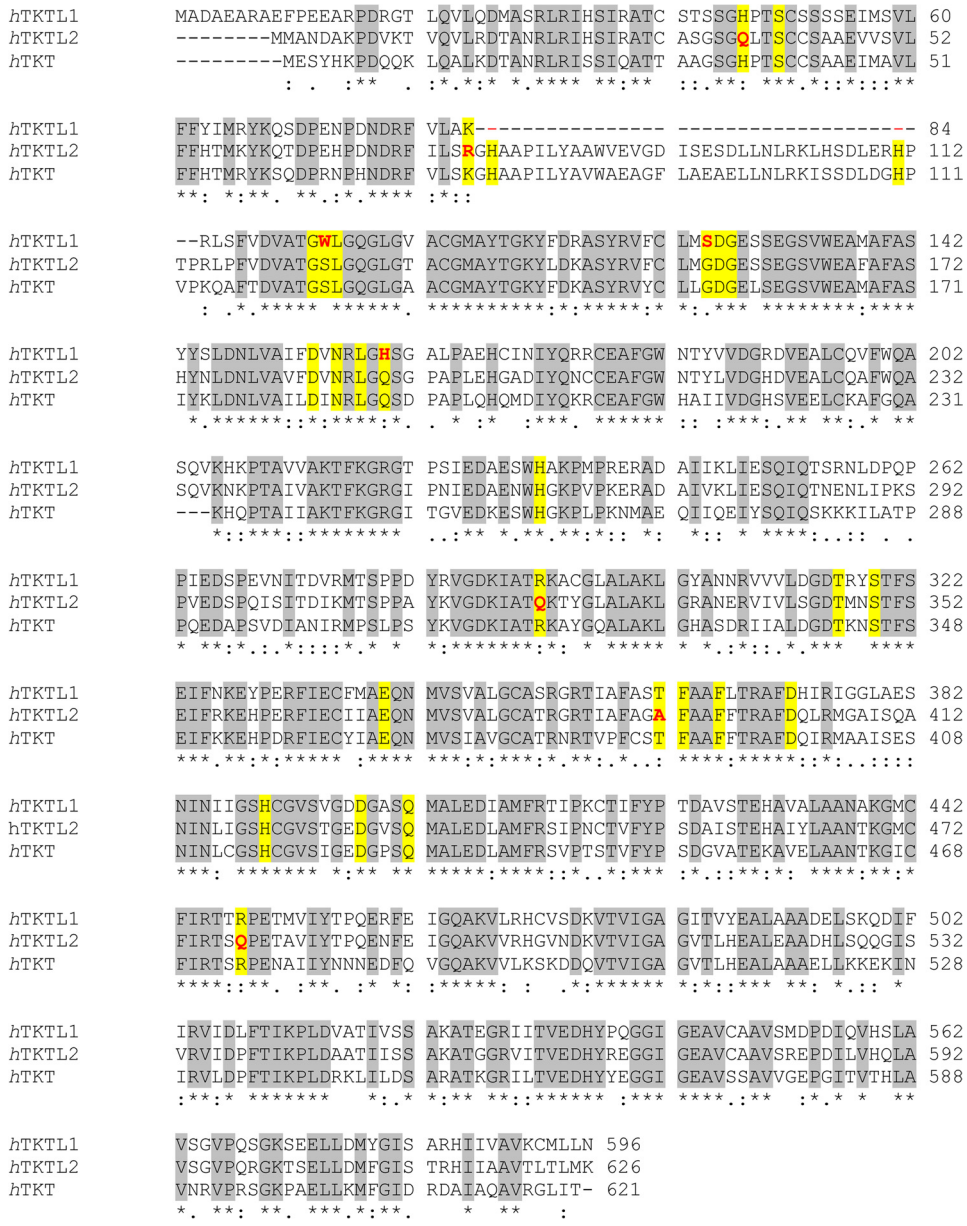

FIGURE 7. **Sequence alignment of human TKT, TKTL1, and TKTL2 (*h*TKT, *h*TKTL1, and *h*TKTL2).** Residues *highlighted* in *gray* are invariant among all three proteins. Residues involved in cofactor and/or substrate binding are *highlighted* in *yellow*. Residues invoked in substrate binding and catalysis in TKT but not conserved in TKTL1 or TKTL2 are indicated in *red*. Sequences were aligned with ClustalW2.

TKT) found to be invariant in all non-mammalian TKTs. This finding rules out the possibility that this residue acts as a general acid/base catalyst and rather suggests a role for substrate binding and orbital alignment in intermediates. Second, residue Gln^{189} sitting atop the thiazolium nucleus as a backstop replaces an isoleucine found in most non-mammalian TKTs. Gln^{189} but not the equivalent isoleucine in non-mammalian TKTs partially occludes the thiazolium ring, inviting speculation that this Gln residue could sterically hinder cofactor dissociation, thus explaining the quasi-irreversible binding of ThDP in mammalian enzymes. Third, the human enzyme contains a lysine residue (Lys^{260}), which is located at the entrance to the substrate channel and is presumably involved in binding of the substrate phosphate. There is no equivalent residue found in non-mammalian TKTs.

Sequence Alignment of Transketolase and Transketolase-like Proteins 1 and 2 and Implications for Putative Functions—Besides TKT, the human genome encodes for the two sequence-wise closely related proteins, TKTL1 and TKTL2, which share a sequence identity on the amino acid level of 61% (TKTL1) and of 66% (TKTL2) compared with TKT. Although the enzymatic function of TKT is well characterized, much less is known about the biochemical and enzymatic properties of TKTL1 and TKTL2. To date, there are no reports on enzymatic or cellular functions of TKTL2. The elucidation of the cellular function of TKTL1 is of particular interest because overexpression of TKTL1 mRNA and protein were observed in different human cancers and have been linked to metastasis and poor survival of cancer patients (29, 44). In contrast to TKTL1, TKT and TKTL2 are not overexpressed in tumor cells, indicating a func-

tional divergence of TKTL1 compared with TKT and TKTL2 (45). The TKTL1 gene is activated by promoter hypomethylation and contributes to carcinogenesis through increased aerobic glycolysis and stabilization of HIF1α (46). Through this stabilization, TKTL1 leads to a shift from a mitochondria-based oxidative energy release to a fermentative energy release concomitant with a suppression of radical- and apoptosis-induced cell death (29). The protective function of TKTL1 in normal cells by reactive oxygen species detoxification and prevention of tissue damage has been demonstrated using TKTL1-deficient mice.[4] Despite these differences from TKT, TKTL1 expression has been shown to compensate for inhibition of TKT translation, thereby restoring cancer drug resistance to imatinib (47).

Based on the newly determined crystal structure of human TKT and a sequence alignment between TKT, TKTL1, and TKTL2, we have analyzed whether amino acid residues shown to be involved in cofactor and substrate binding in TKT are also conserved in TKTL1 and -2 (Fig. 7). As mentioned before, TKTL1 has a deletion of 38 amino acids in the N-terminal PP domain (residues 76–113 in TKT). This segment folds into a loop-helix-turn-helix-loop motif in human TKT. Both loop regions constitute part of the active and cofactor binding site and harbor numerous residues that are likely to play important roles for cofactor binding (His^{77}) and catalysis (His^{77}/His^{110}). Both residues are invariant in all TKTs, and the homologous residues of His^{110} in yeast and bacterial TKT were shown to form an essential hydrogen-bonding interaction with 1-OH of the X5P-ThDP, F6P-ThDP, and DHE-ThDP carbanion/enamine intermediates (11, 12). Mutagenesis studies revealed that any substitution of His^{110} renders human TKT inactive (5). In addition, there is a mutation in the GDG (residues 154–156 in TKT) cofactor binding consensus sequence; TKTL1 features a SDG sequence instead. The GDG consensus sequence is highly conserved among all TKTs (4); there is only one annotated sequence in which the first glycine is replaced (TKT from *Mycobacterium leprae*) by another residue. However, the enzymatic function of this particular protein has not been proven experimentally but was inferred from sequence similarity. Another difference in sequence of the putative cofactor binding site is found for Gln^{189}, which serves as a backstop for the thiazolium ring of ThDP in TKT and is replaced by a histidine in TKTL1. A third crucial difference can be identified for a short loop (Gly^{123}-Ser^{124}-Leu^{125}) involved in binding of the aminopyrimidine. In TKTL1, the bulky tryptophan replaces the otherwise highly conserved serine (or proline) residue. Taken together, TKTL1 is lacking several important residues proven to be important for cofactor binding and catalysis in all hitherto characterized TKTs, suggesting that TKTL1 may not possess a common transketolase activity. Moreover, it remains to be studied whether TKTL1 does bind ThDP at all because several critical determinants of cofactor binding in TKTs are either missing in TKTL1 or nonconservatively replaced.

In the sequence of transketolase-like protein 2, there are also several substitutions of residues belonging to the active site and cofactor binding pocket in TKT. Lys^{75} involved in bonding of the diphosphate anchor of ThDP in TKT is conservatively replaced by an arginine residue. However, a histidine (His^{37} in human TKT) and two arginines (Arg^{474} and Arg^{318}), which are totally invariant among all TKTs are non-homologously replaced in TKTL2 by glutamine residues in each case. Structural studies revealed these side chains to interact either with substrate hydroxyl groups (histidine) or with the phosphate moiety (arginines) (10, 12). Substitutions of the invariant histidine abolished activity, whereas binding of phosphorylated sugar substrates is significantly compromised in variants with substitutions of the conserved arginine residues (48, 49). In conclusion, TKTL2 lacks numerous residues that are important for substrate binding and catalysis in TKTs and can thus be expected to possess only little TKT activity if any.

CONCLUSIONS

The crystal structure of human TKT has been determined as the first structure of a mammalian TKT. Although subunit topology, dimer assembly, and active site architecture are highly conserved among all TKTs, mammalian TKTs have evolved numerous unique interactions with the cofactor and the substrate/reaction intermediates. The related proteins TKTL1 and TKTL2 lack numerous invariant residues involved in cofactor and substrate binding and are therefore not expected to possess TKT activity.

Acknowledgment—We thank Dr. C. Göbel for mass spectrometric analysis of chemoenzymatically synthesized S7P.

REFERENCES

1. Schenk, G., Duggleby, R. G., and Nixon, P. F. (1998) *Int. J. Biochem. Cell Biol.* **30,** 1297–1318
2. Schneider, G., and Lindqvist, Y. (1998) *Biochim. Biophys. Acta* **1385,** 387–398
3. Kluger, R., and Tittmann, K. (2008) *Chem. Rev.* **108,** 1797–1833
4. Schenk, G., Layfield, R., Candy, J. M., Duggleby, R. G., and Nixon, P. F. (1997) *J. Mol. Evol.* **44,** 552–572
5. Singleton, C. K., Wang, J. J., Shan, L., and Martin, P. R. (1996) *Biochemistry* **35,** 15865–15869
6. Lindqvist, Y., Schneider, G., Ermler, U., and Sundström, M. (1992) *EMBO J.* **11,** 2373–2379
7. Nikkola, M., Lindqvist, Y., and Schneider, G. (1994) *J. Mol. Biol.* **238,** 387–404
8. Littlechild, J., Turner, N., Hobbs, G., Lilly, M., Rawas, A., and Watson, H. (1995) *Acta. Crystallogr. D Biol. Crystallogr.* **51,** 1074–1076
9. Gerhardt, S., Echt, S., Busch, M., Freigang, J., Auerbach, G., Bader, G., Martin, W. F., Bacher, A., Huber, R., and Fischer, M. (2003) *Plant Physiol.* **132,** 1941–1949
10. Nilsson, U., Meshalkina, L., Lindqvist, Y., and Schneider, G. (1997) *J. Biol. Chem.* **272,** 1864–1869
11. Fiedler, E., Thorell, S., Sandalova, T., Golbik, R., König, S., and Schneider, G. (2002) *Proc. Natl. Acad. Sci. U.S.A.* **99,** 591–595
12. Asztalos, P., Parthier, C., Golbik, R., Kleinschmidt, M., Hübner, G., Weiss, M. S., Friedemann, R., Wille, G., and Tittmann, K. (2007) *Biochemistry* **46,** 12037–12052
13. Tittmann, K., and Wille, G. (2009) *J. Mol. Catal. B Enzym.* **61,** 93–99
14. Nixon, P. F., Kaczmarek, M. J., Tate, J., Kerr, R. A., and Price, J. (1984) *Eur. J. Clin. Invest.* **14,** 278–281
15. Héroux, M., Raghavendra Rao, V. L., Lavoie, J., Richardson, J. S., and Butterworth, R. F. (1996) *Metab. Brain Dis.* **11,** 81–88
16. Hammes, H. P., Du, X., Edelstein, D., Taguchi, T., Matsumura, T., Ju, Q.,

[4] S. Bentz, T. Pesch, L. Wolfram, C. de Valliere, K. Leucht, M. Fried, J. Coy, M. Hausmann, and G. Rogler, submitted for publication.

Lin, J., Bierhaus, A., Nawroth, P., Hannak, D., Neumaier, M., Bergfeld, R., Giardino, I., and Brownlee, M. (2003) *Nat. Med.* **9,** 294–299
17. Zhao, Y., Pan, X., Zhao, J., Wang, Y., Peng, Y., and Zhong, C. (2009) *J. Neurochem.* **111,** 537–546
18. Liu, S., Sun, M. Z., Tang, J. W., Wang, Z., Sun, C., and Greenaway, F. T. (2008) *Rapid Commun. Mass Spectrom.* **22,** 3172–3178
19. Cascante, M., Centelles, J. J., Veech, R. L., Lee, W. N., and Boros, L. G. (2000) *Nutr. Cancer* **36,** 150–154
20. Shin, Y. K., Yoo, B. C., Hong, Y. S., Chang, H. J., Jung, K. H., Jeong, S. Y., and Park, J. G. (2009) *Electrophoresis* **30,** 2182–2192
21. Xu, Z. P., Wawrousek, E. F., and Piatigorsky, J. (2002) *Mol. Cell. Biol.* **22,** 6142–6147
22. Calingasan, N. Y., Sheu, K. F., Baker, H., Jung, E. H., Paoletti, F., and Gibson, G. E. (1995) *J. Neurochem.* **64,** 1034–1044
23. Sax, C. M., Salamon, C., Kays, W. T., Guo, J., Yu, F. X., Cuthbertson, R. A., and Piatigorsky, J. (1996) *J. Biol. Chem.* **271,** 33568–33574
24. Boros, L. G., Puigjaner, J., Cascante, M., Lee, W. N., Brandes, J. L., Bassilian, S., Yusuf, F. I., Williams, R. D., Muscarella, P., Melvin, W. S., and Schirmer, W. J. (1997) *Cancer Res.* **57,** 4242–4248
25. Thomas, A. A., De Meese, J., Le Huerou, Y., Boyd, S. A., Romoff, T. T., Gonzales, S. S., Gunawardana, I., Kaplan, T., Sullivan, F., Condroski, K., Lyssikatos, J. P., Aicher, T. D., Ballard, J., Bernat, B., DeWolf, W., Han, M., Lemieux, C., Smith, D., Weiler, S., Wright, S. K., Vigers, G., and Brandhuber, B. (2008) *Bioorg. Med. Chem. Lett.* **18,** 509–512
26. Thomas, A. A., Le Huerou, Y., De Meese, J., Gunawardana, I., Kaplan, T., Romoff, T. T., Gonzales, S. S., Condroski, K., Boyd, S. A., Ballard, J., Bernat, B., DeWolf, W., Han, M., Lee, P., Lemieux, C., Pedersen, R., Pheneger, J., Poch, G., Smith, D., Sullivan, F., Weiler, S., Wright, S. K., Lin, J., Brandhuber, B., and Vigers, G. (2008) *Bioorg. Med. Chem. Lett.* **18,** 2206–2210
27. Le Huerou, Y., Gunawardana, I., Thomas, A. A., Boyd, S. A., de Meese, J., Dewolf, W., Gonzales, S. S., Han, M., Hayter, L., Kaplan, T., Lemieux, C., Lee, P., Pheneger, J., Poch, G., Romoff, T. T., Sullivan, F., Weiler, S., Wright, S. K., and Lin, J. (2008) *Bioorg. Med. Chem. Lett.* **18,** 505–508
28. Coy, J. F., Dübel, S., Kioschis, P., Thomas, K., Micklem, G., Delius, H., and Poustka, A. (1996) *Genomics* **32,** 309–316
29. Xu, X., Zur Hausen, A., Coy, J. F., and Löchelt, M. (2009) *Int. J. Cancer* **124,** 1330–1337
30. Charmantray, F., Helaine, V., Legeret, B., and Hecquet, L. (2009) *J Mol. Catal. B Enzym.* **57,** 6–9
31. Bykova, I. A., Solovjeva, O. N., Meshalkina, L. E., Kovina, M. V., and Kochetov, G. A. (2001) *Biochem. Biophys. Res. Commun.* **280,** 845–847
32. Tittmann, K., Golbik, R., Uhlemann, K., Khailova, L., Schneider, G., Patel, M., Jordan, F., Chipman, D. M., Duggleby, R. G., and Hübner, G. (2003) *Biochemistry* **42,** 7885–7891
33. Schneider, G., Sundström, M., and Lindqvist, Y. (1989) *J. Biol. Chem.* **264,** 21619–21620
34. Kabsch, W. (1993) *J. Appl. Crystallogr.* **26,** 795–800
35. Collaborative Computational Project 4 (1994) *Acta Crystallogr. D Biol. Crystallogr.* **50,** 760–763
36. Emsley, P., and Cowtan, K. (2004) *Acta Crystallogr. D Biol. Crystallogr.* **60,** 2126–2132
37. Davis, I. W., Leaver-Fay, A., Chen, V. B., Block, J. N., Kapral, G. J., Wang, X., Murray, L. W., Arendall, W. B., 3rd, Snoeyink, J., Richardson, J. S., and Richardson, D. C. (2007) *Nucleic Acids Res.* **35,** W375–W383
38. Thompson, J. D., Gibson, T. J., and Higgins, D. G. (2002) *Current Protocols in Bioinformatics*, Chapter 2, Unit 2.3, John Wiley & Sons, Inc., New York
39. Gouet, P., Courcelle, E., Stuart, D. I., and Métoz, F. (1999) *Bioinformatics* **15,** 305–308
40. Schenk, G., Duggleby, R. G., and Nixon, P. F. (1998) *Int. J. Biochem. Cell Biol.* **30,** 369–378
41. Sprenger, G. A., Schörken, U., Sprenger, G., and Sahm, H. (1995) *Eur. J. Biochem.* **230,** 525–532
42. Holm, L., Kääriäinen, S., Rosenström, P., and Schenkel, A. (2008) *Bioinformatics* **24,** 2780–2781
43. Hawkins, C. F., Borges, A., and Perham, R. N. (1989) *FEBS Lett.* **255,** 77–82
44. Furuta, E., Okuda, H., Kobayashi, A., and Watabe, K. (2010) *Biochim. Biophys. Acta Rev. Cancer* **1805,** 141–152
45. Sigrun, L., Zerilli, M., Zur, H. A., Popa, J., Steidler, A., Alken, P., Stassi, G., Schubert, P., and Coy, J. F. (2006) *Tumor Biol.* **27,** 48–48
46. Sun, W., Liu, Y., Glazer, C. A., Shao, C., Bhan, S., Demokan, S., Zhao, M., Rudek, M. A., Ha, P. K., and Califano, J. A. (2010) *Clin. Cancer Res.* **16,** 857–866
47. Zhao, F., Mancuso, A., Bui, T. V., Tong, X., Gruber, J. J., Swider, C. R., Sanchez, P. V., Lum, J. J., Sayed, N., Melo, J. V., Perl, A. E., Carroll, M., Tuttle, S. W., and Thompson, C. B. (2010) *Oncogene* **29,** 2962–2972
48. Wikner, C., Nilsson, U., Meshalkina, L., Udekwu, C., Lindqvist, Y., and Schneider, G. (1997) *Biochemistry* **36,** 15643–15649
49. Soh, Y., Song, B. J., Jeng, J., and Kallarakal, A. T. (1998) *Biochem. J.* **333,** 367–372